

Pursuing Colloidal Diamond Supporting Information

Łukasz Baran, Dariusz Tarasewicz, Daniel M. Kamiński, Wojciech Rżysko

1 Justification of the chosen model

Model used throughout the current study, was similar as already reported in our previous papers [1, 2]. We found that the choice of the model parameters to be $\sigma_a = 0.2\sigma$, $\varepsilon_{aa} = 5.0\varepsilon$, and $r_{cut} = 2\sigma_a$ is the most efficient to describe relatively strong but reversible associative interactions. The parameter l allows one to the precise control over the desired patch's valency. In order to study diamond phases, we found that $l = 0.36\sigma$ allows for single association of each active sites, resulting in the formation of the total of four bonds per particle. To demonstrate that, Figure S1 displays the distribution of a number of nearest neighbors N_{nn} per particle for three different embedment distances being $l = 0.36\sigma$, $l = 0.40\sigma$, and $l = 0.45\sigma$, calculated up to the first minimum in the radial distribution function $r_{max} = 1.2\sigma$.

One can see that $N_{nn} = 4$ dominates for $l = 0.36\sigma$ and $l = 0.40\sigma$, however, in the case of the latter we see that it can take values between 5 – 7 indicating the possibility that a patch can have higher valency than one. Systems with $l = 0.45\sigma$ take values of $N_{nn} = 9, 12$ as the most probable, indicating the possibility for the formation of fcc/hcp-like crystalline networks which was beyond the scope of current study.

2 Bulk phase diagram

As mentioned in the main text, the phase diagram has been evaluated using block's analysis method proposed by Binder [3]. The distribution functions for several distinct densities and different temperatures are shown in Fig. S2. Part (a) display a regular distribution exhibiting double-peak behavior corresponding to the two-phase coexistence. In present case, we are dealing with the gas-solid coexistence, the latter phase being an hybrid of interwoven hexagonal and cubic diamond polymorphs at around $\rho = 0.71$.

In part (b), on the other hand, one can see that at temperature $T^* = 0.305$ and the density $\rho = 0.4$, there is a gaussian peak, indicating disordered fluid, that is uniformly distributed over an entire system space. This means that in such conditions, we are above the transition temperature into the ordered phase. The same concerns higher densities, however, it needs to be emphasized that suitable transition temperature accordingly increases.

In part (c), we observe large peak around $\rho = 0.71$ corresponding to diamond phases as previously. On the other hand, the low-density peaks vanished which corroborate that gas-solid coexistence is not present under such circumstances. Strikingly, other peaks with slightly lower density than the crystalline phase appear. We conjecture that this is due to the presence of a liquid phase that emerges in a relatively narrow region. Moreover, we did not observe fluctuations between gas and liquid phase within this range of temperatures and for all densities studied, therefore, we envisage this liquid phase is metastable.

In part (d), at higher density, we observe the coexistence between diamond phases and BCC, the latter of which is composed of two interwoven diamond phases. Presence of BCC and other phases has been evaluated by means of the calculation Steinhard order parameter (Eq. 2 and 3 in the main text). The criteria for the discrimination of particular crystalline environments can be found in Table I of the following article [4]. Corresponding snapshots for densities

$\rho = 1.0$ and $\rho = 1.2$ are displayed in Figure S3. In view of all the above, this phase diagram is of a similar type as the ones reported by Romano *et al.* [5, 6], although performed for different interparticle potential.

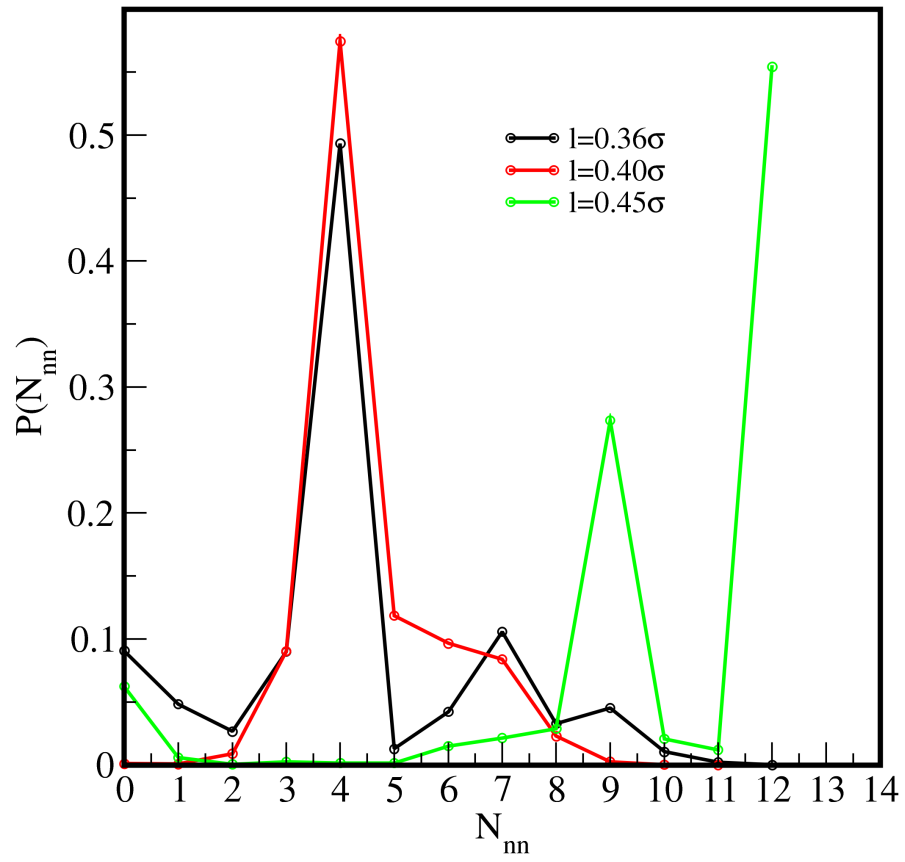


Figure S1: The distribution of the nearest neighbors for systems differing in the embedding distance l .

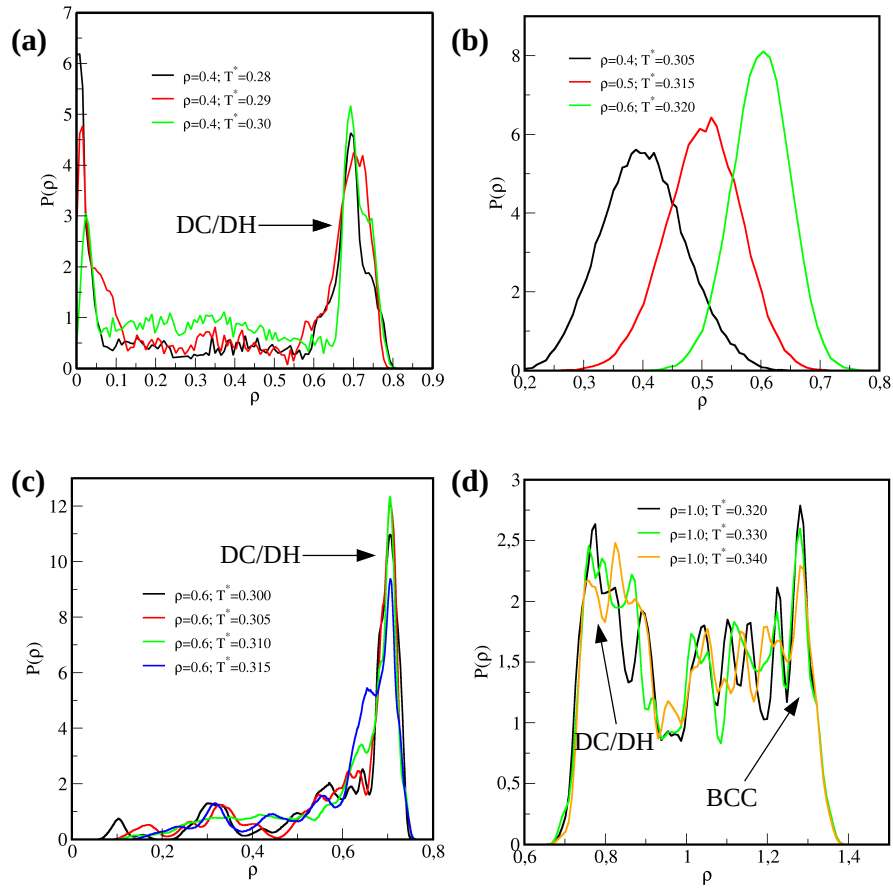


Figure S2: The density distribution functions of the largest block for bulk systems at different densities and temperatures.

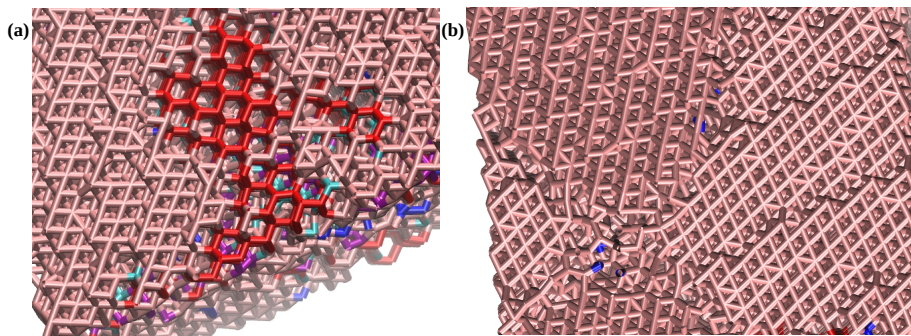


Figure S3: Fragment of the configurations for systems in $\rho = 1.0$ (a) and $\rho = 1.2$ (b) at $T = 0.34$. Red sticks correspond to cubic diamond whereas pink sticks is the remaining fluid.

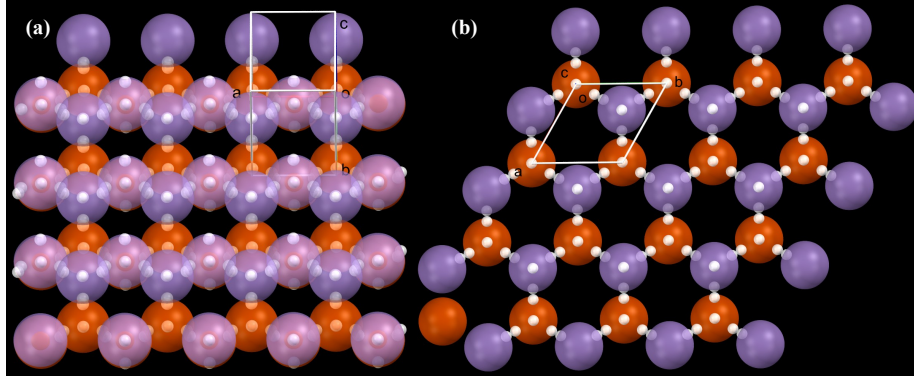


Figure S4: Fragment of the configurations of (a): (110) and (b):(111) faces of cubic diamond formed by tetrahedral patchy particles for systems $\xi = 1.0$ (a) and $\xi = 0.4$ (b). Yellow and purple atoms correspond to the lower and upper layer, respectively. White spheres schematically represent the active sites.

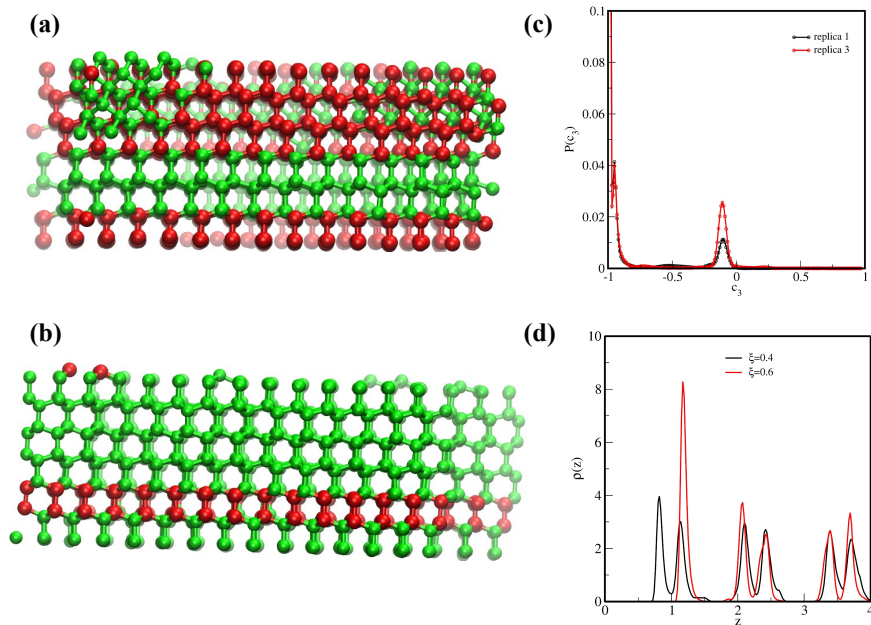


Figure S5: Parts (a, b): Snapshots of two different replicas, differing in the ratio of two cubic polymorphs in the stacking hybrids. Part (c): Distribution function of the order parameter $P(c_3)$ for replicas shown in parts (a, b). Part (d): Comparison of density profiles for $\xi = 0.4$ and $\xi = 0.6$. The latter is shifted by $1/3\sigma$ in the z -direction (cf. Main text).

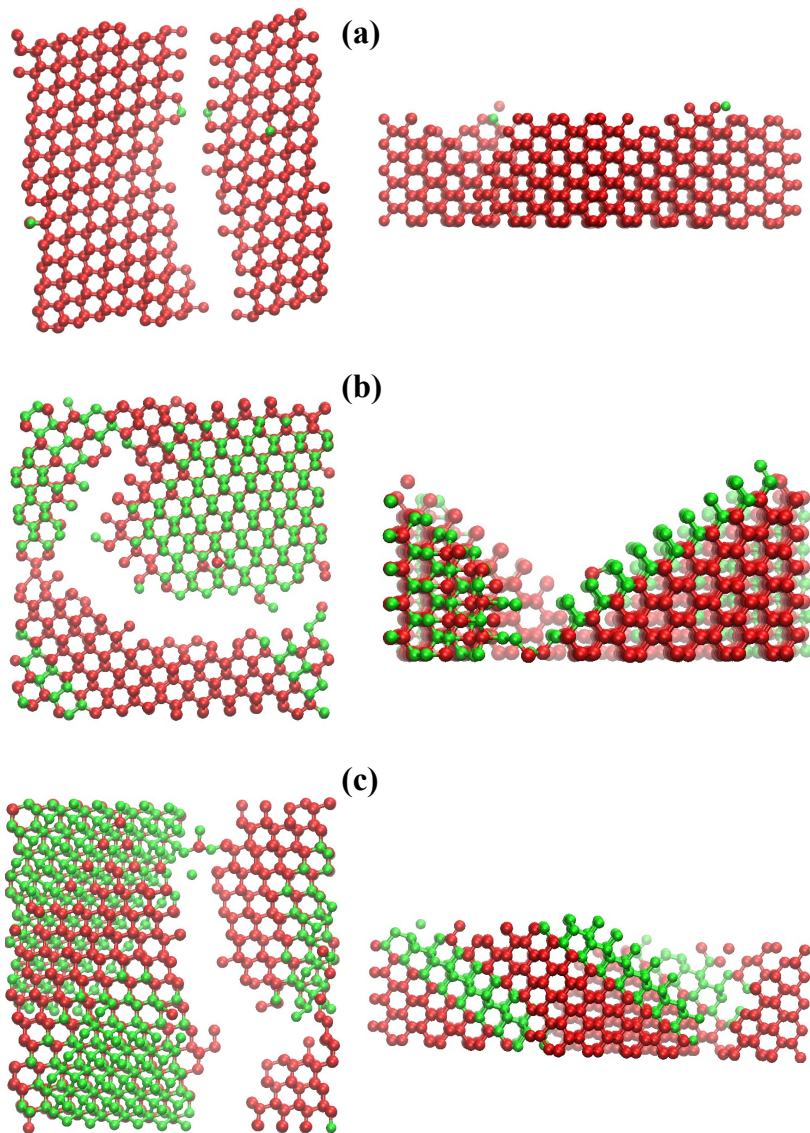


Figure S6: Snapshots for three different replicas for system $\xi = 1.0$ at $T^* = 0.30$. Left and right panels correspond to top and front view, respectively.

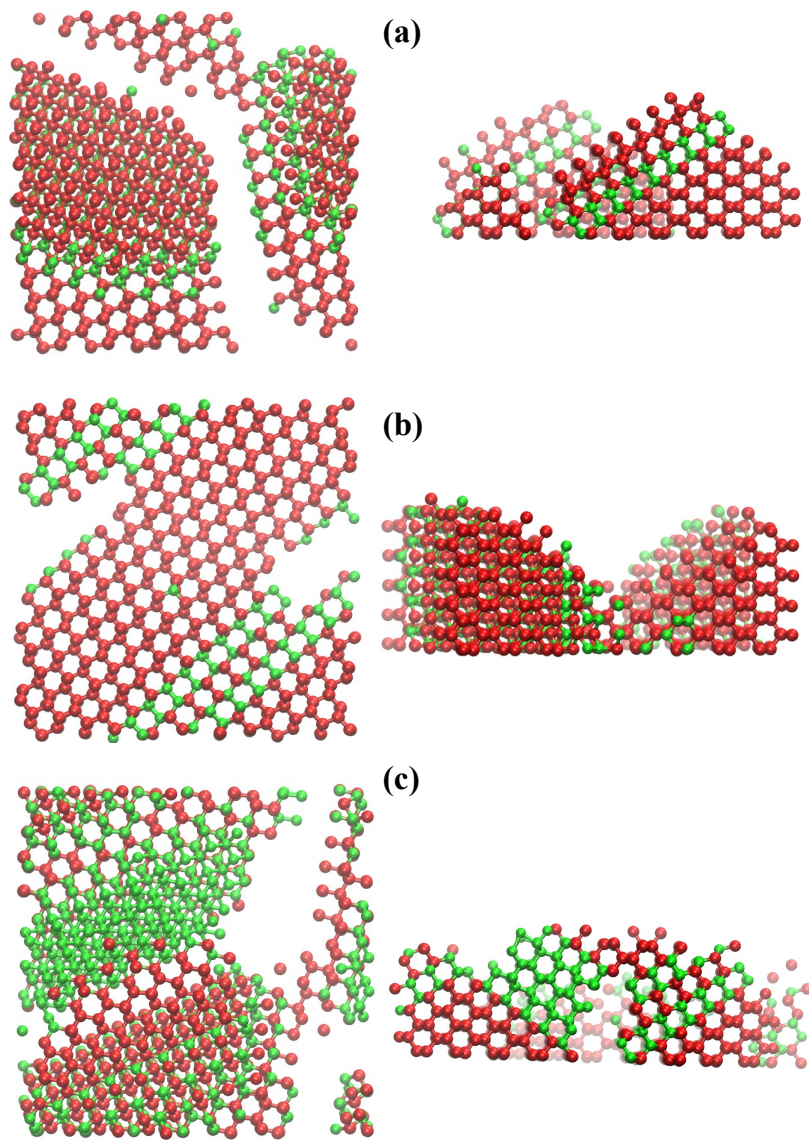


Figure S7: Snapshots for three different replicas for system $\xi = 1.2$ at $T^* = 0.30$. Left and right panels correspond to top and front view, respectively.

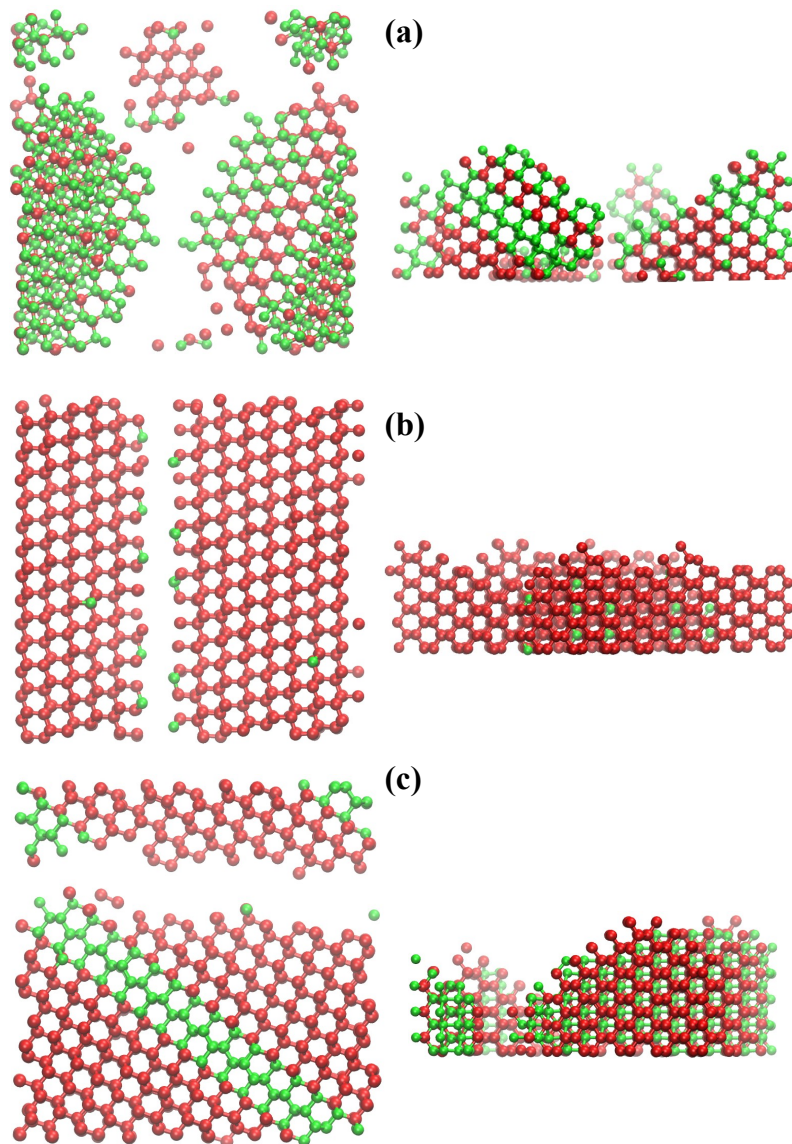


Figure S8: Snapshots for three different replicas for system $\xi = 1.4$ at $T^* = 0.30$. Left and right panels correspond to top and front view, respectively.

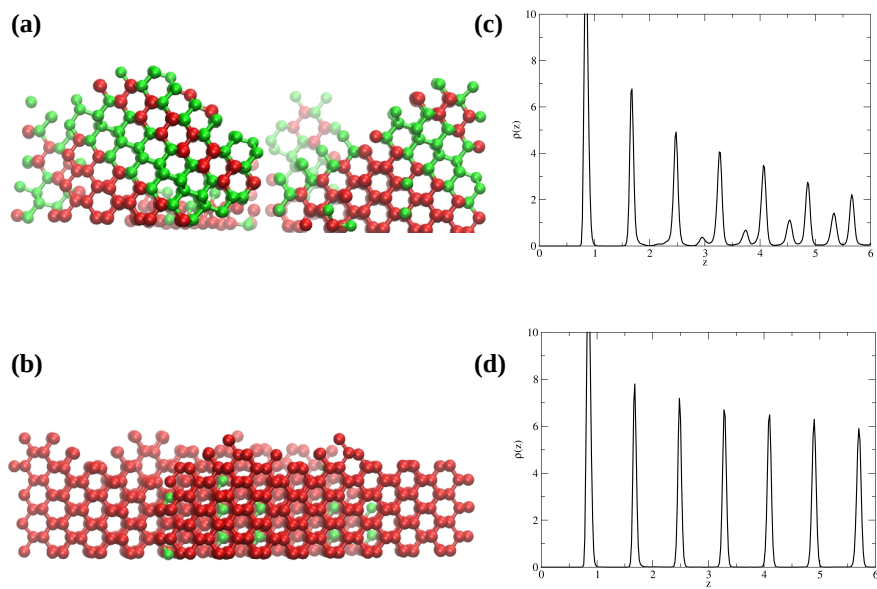


Figure S9: Parts (a, b): Snapshots for two different replicas for system $\xi = 1.4$ at $T^* = 0.30$. Parts (c, d): Density profiles for replicas shown in parts (a, b) with tilted (c) and flat growth of the crystal (d).

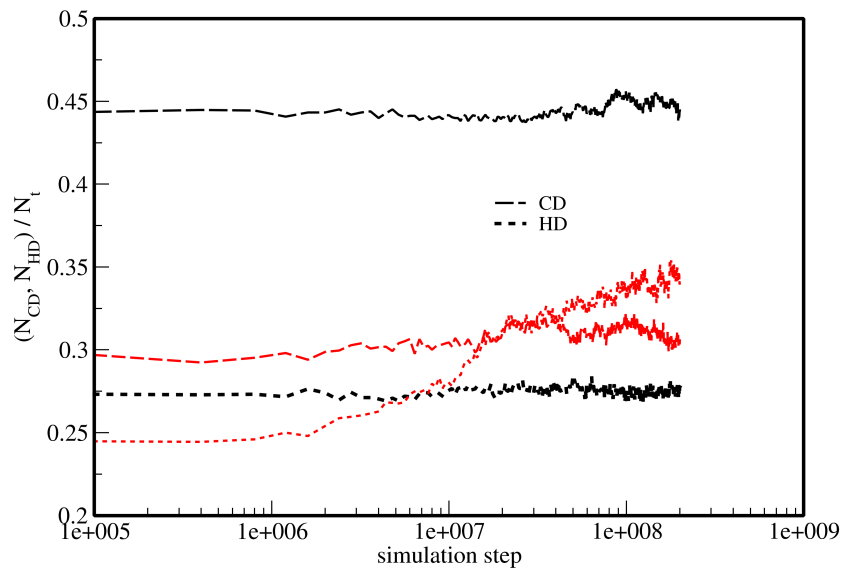


Figure S10: The time evolution of the number of patchy particles belonging to CD and HD networks when the external field is removed for $\xi = 0.4$, $T^* = 0.29$ (black lines) and $\xi = 0.6$, $T^* = 0.29$ (red lines)

References

- [1] Ł. Baran and W. Rżysko, “Application of a coarse-grained model for the design of complex supramolecular networks,” *Mol. Syst. Des. Eng.*, vol. 5, pp. 484–492, 2020.
- [2] Ł. Baran, W. Rżysko, and D. Tarasewicz, “Variation of interaction zone size for the target design of 2d supramolecular networks,” *Mol. Syst. Des. Eng.*, vol. 6, pp. 805–816, 2021.
- [3] K. Binder, “Finite size scaling analysis of ising model block distribution functions,” *Zeitschrift für Physik B Condensed Matter*, vol. 43, pp. 119–140, 1981.
- [4] W. Mickel, S. C. Kapfer, G. E. Schröder-Turk, and K. Mecke, “Shortcomings of the bond orientational order parameters for the analysis of disordered particulate matter,” *The Journal of Chemical Physics*, vol. 138, no. 4, p. 044501, 2013.
- [5] F. Romano, E. Sanz, and F. Sciortino, “Crystallization of tetrahedral patchy particles in silico,” *The Journal of Chemical Physics*, vol. 134, no. 17, p. 174502, 2011.
- [6] F. Romano, E. Sanz, and F. Sciortino, “Phase diagram of a tetrahedral patchy particle model for different interaction ranges,” *The Journal of Chemical Physics*, vol. 132, no. 18, p. 184501, 2010.